JACS
JOURNAL OF THE AMERICAN CHEMICAL SOCIETY
Article
pubs.acs.org/JACS

Synthesis of Quinoidal Fused Oligosiloles by Rhodium-Catalyzed Stitching Reaction and Theoretical Investigation of Their Properties

Ryo Shintani,*[,†] Nana Misawa,[†,§] Tomohiro Tsuda,[†,§] Ryo Iino,[†] Mikiya Fujii,[‡] Koichi Yamashita,*[,‡] and Kyoko Nozaki*[,†]

[†]Department of Chemistry and Biotechnology, Graduate School of Engineering, The University of Tokyo, 7-3-1 Hongo, Bunkyo-ku, Tokyo 113-8656, Japan

[‡]Department of Chemical System Engineering, School of Engineering, The University of Tokyo, 7-3-1 Hongo, Bunkyo-ku, Tokyo 113-8656, Japan

Supporting Information

ABSTRACT: New quinoidal fused oligosiloles containing an even number of silole units have been synthesized by a rhodium-catalyzed stitching reaction. Employing $[RhCl(tfb)]_2$ as the catalyst significantly improved the stitching efficiency, and up to six siloles could be fused in quinoidal form. A systematic comparison of the physical properties of **Si1**−**Si6**′ confirmed the unique trend in their LUMO levels, which become higher with longer π conjugation. To understand the origin of this unusual trend, theoretical calculations were also carried out using various model compounds, and the results indicated that the terminal indenylidene (cyclopentadienylidene) moieties in **Si1**−**Si6** (**Si1a**−**Si6a**) are primarily responsible for this phenomenon through their frontier orbital correlations with the HOMO of the central polyene unit, which becomes higher in energy with longer π conjugation.

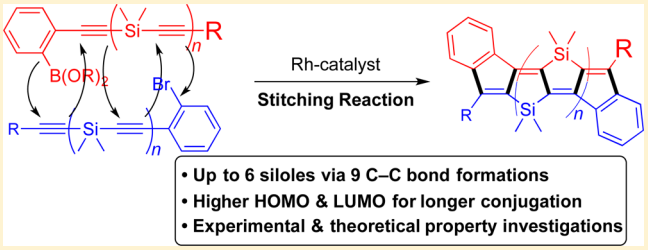

INTRODUCTION

Silicon-bridged π-conjugated compounds are being intensively investigated as potentially useful functional organic materials because of their optoelectronic properties. The most typical structures of this class of compounds are silicon-bridged (hetero)biaryls such as dibenzosiloles[1] and dithienosiloles,[2] and these compounds are usually synthesized from the corresponding nonbridged ortho-dihalogenated (hetero)biaryls through metal−halogen exchange and successive introduction of a bridging silicon atom by the reaction with a dichlorosilane.[3] In contrast to these widely studied (hetero)biaryl-based structures, investigations of other types of silicon-bridged π-conjugated compounds are quite limited,[4] presumably mainly as a result of the lack of efficient synthetic methods. To further enhance the utility of silicon-bridged π-conjugated compounds in the field of materials science, it is therefore highly important to develop a new synthetic method that provides facile access to a new structural motif. In this regard, we recently developed a novel synthetic approach, a rhodium-catalyzed stitching reaction between two different oligo(silylene ethynylene)s, and successfully synthesized a series of quinoidal fused oligosiloles in a convergent manner.[5−7] We also found that these compounds exhibit an unusual trend in their LUMO levels, which become higher with longer π conjugation. However, the origin of this trend has not been elucidated.

The original design of substrates for this stitching reaction inherently leads to the formation of quinoidal fused oligosiloles containing an odd number of silole units because of the use of a compound containing both the start point (arylboronate) and the end point (aryl halide) as one of the reaction partners (Scheme 1a). In this article, we describe the development of a synthetic method for quinoidal fused oligosiloles containing an even number of silole units by proper modification of the substrate design (Scheme 1b) and a comparison of their physical properties with those of the previously synthesized compounds. We also theoretically investigate the origin of the observed unusual LUMO trend of these quinoidal fused oligosiloles.

RESULTS AND DISCUSSION

1. Synthesis of New Quinoidal Fused Oligosiloles. On the basis of our previous success in the synthesis of quinoidal fused oligosiloles containing an odd number of silole units (Scheme 1a), we envisioned that analogous quinoidal fused oligosiloles containing an even number of silole units could be synthesized by employing a substrate combination of an arylboronate-terminated oligo(silylene ethynylene) and a bromoarene-terminated oligo(silylene ethynylene) with equal lengths (Scheme 1b). To put this idea into practice, we initially focused on the synthesis of compounds **3** having two silole units (Table 1). At first, we conducted a reaction of arylboronate **1a** and bromoarene **2a**, both of which contain a 1-propynyl group on the silicon atom (entry 1), under the conditions previously used for the synthesis of **Si1** and **Si3** in the presence of 8 mol % Rh/cod catalyst.[5] As a result, although

Received: January 11, 2017
Published: February 22, 2017

DOI: 10.1021/jacs.7b00344
J. Am. Chem. Soc. 2017, 139, 3861−3867

Scheme 1. (a) Recently Developed Rhodium-Catalyzed Stitching Reaction To Give Quinoidal Fused Oligosiloles with an Odd Number of Silole Units (Si1, Si3, and Si5); (b) Newly Designed Rhodium-Catalyzed Stitching Reaction To Give Quinoidal Fused Oligosiloles with an Even Number of Silole Units

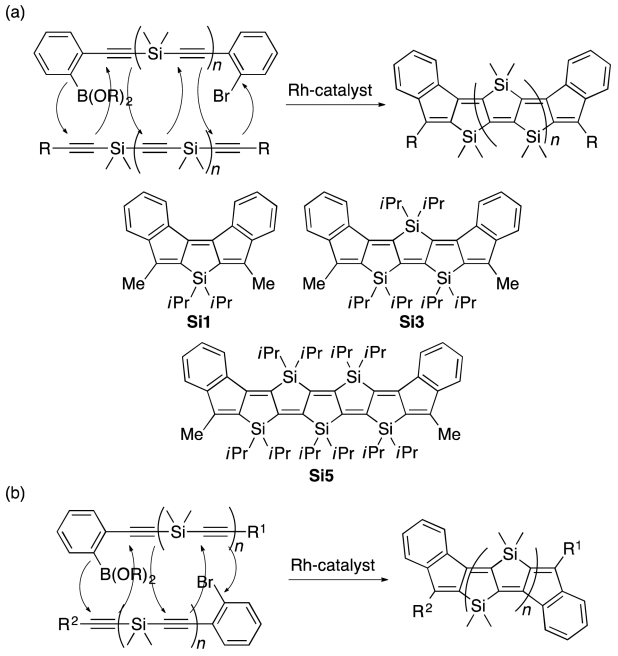

Table 1. Rhodium-Catalyzed Stitching Reaction of 1 with 2

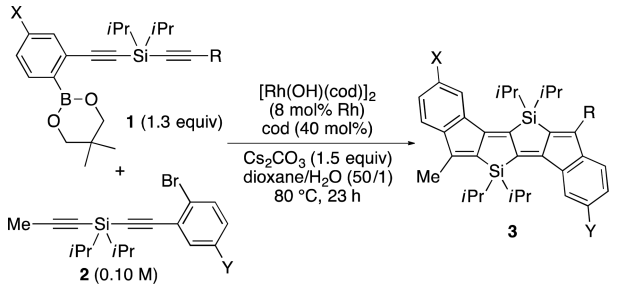

entry	1	2	product	yield (%)[a]
1	**1a** (R = Me, X = H)	**2a** (Y = H)	**3aa** (**Si2**)	17
2[b]	**1a**	**2a**	**3aa**	42
3	**1b** (R = Ph, X = H)	**2a**	**3ba**	72
4	**1c** (R = *t*Bu, X = H)	**2a**	**3ca** (**Si2′**)	74
5	**1d** (R = *t*Bu, X = Cl)	**2b** (Y = Cl)	**3db**	57
6[b]	**1e** (R = *t*Bu, X = NMe_2)	**2c** (Y = NO_2)	**3ec**	64

[a]Isolated yields. [b]The reaction was conducted with 20 mol % rhodium catalyst.

the desired compound **3aa** (**Si2**) was obtained, the yield was only 17%, with significant amounts of remaining substrates (0.50 equiv of **1a** and 79% of **2a**). The yield of **3aa** could be somewhat improved to 42% by increasing the catalyst loading (20 mol % Rh) with almost full consumption of **1a** and 50% of the remaining **2a** (entry 2). These results may indicate that differentiation of the terminal substituents on the alkynes of **1** and **2** is necessary to achieve a highly selective stitching reaction to give quinoidal fused oligosiloles **3** more efficiently (Scheme 2).[8] On the basis of this hypothesis, we decided to introduce a bulkier group on the alkyne of **1** while keeping the terminal

Scheme 2. Desired and Undesired Carborhodation Pathways during the Stitching Reaction of 1a with 2a

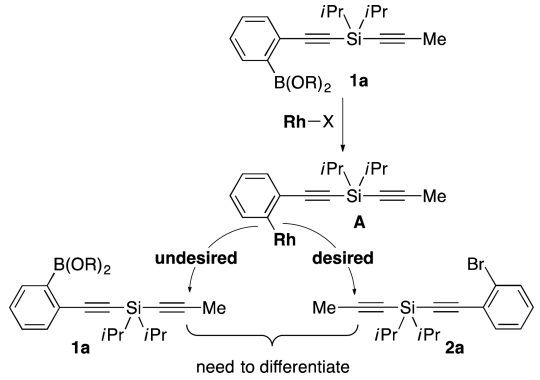

substituent of **2** as methyl to facilitate selective insertion of **2** into the arylrhodium species generated from **1**. Indeed, the use of arylboronate **1b** (R = Ph) or **1c** (R = *t*Bu) in combination with bromoarene **2a** significantly improved the yield of **3** to 72–74% under the same conditions as employed in entry 1 (**3ba** and **3ca** (**Si2′**), respectively; entries 3 and 4). Functionalized compounds **3** could also be prepared by the present stitching reaction using the combination of functionalized compounds **1** with a *tert*-butyl group on the alkyne and **2** with a methyl group on the alkyne. For example, dichlorinated compound **3db** was obtained in 57% yield, which could potentially be further functionalized using the rich chemistry of aryl halides such as cross-coupling, homocoupling, and metal–halogen exchange (entry 5). In addition, the donor–acceptor-type compound **3ec** having dimethylamino and nitro groups at the terminals of π conjugation was synthesized in 64% yield, although a higher catalyst loading (20 mol % Rh) was required (entry 6).

We also applied the present stitching reaction to the synthesis of longer quinoidal fused oligosilole **Si4′** containing four silole units through the formation of seven consecutive carbon–carbon bonds. As shown in eq 1, however, the reaction

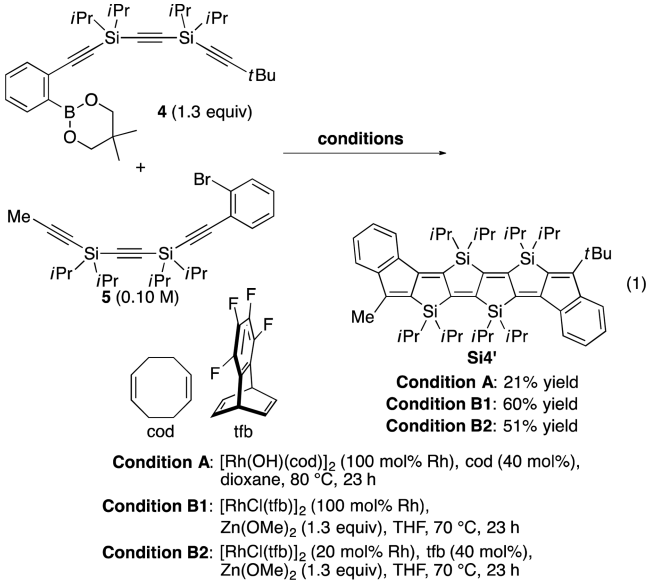

(1)

of substrates **4** and **5** gave only a 21% yield of **Si4′** even in the presence of a stoichiometric amount of the Rh/cod complex (condition A). We subsequently found that the yield of **Si4′**

DOI: 10.1021/jacs.7b00344
J. Am. Chem. Soc. 2017, 139, 3861–3867

could be significantly improved to 60% by using a stoichiometric amount of a Rh/tfb complex (condition B1), and even the use of a catalytic amount of Rh/tfb (20 mol % Rh) led to the formation of **Si4′** in a reasonably high yield of 51% (condition B2).[9] The Rh/tfb catalyst system was found to be superior to the Rh/cod catalyst system for the synthesis of an even longer quinoidal fused oligosilole. Thus, as shown in eq 2, in the presence of a stoichiometric amount of $[RhCl(tfb)]_2$

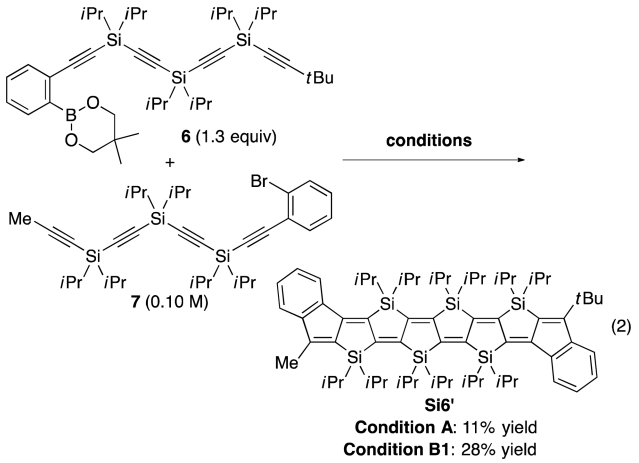

(condition B1), **Si6′** having six silicon atoms could be synthesized in 28% yield from substrates **6** and **7** through the formation of nine carbon−carbon bonds, whereas only an 11% yield of **Si6′** was obtained using the Rh/cod complex (condition A). It is also worth noting that this result represents the synthesis of the longest quinoidal fused oligoheterole to date as far as we are aware.

2. Physical Properties of Quinoidal Fused Oligosiloles.

2-1. Substituent Effect of Compounds 3 (Si2). With a series of new quinoidal fused oligosiloles in hand, we initially examined the optical and electronic properties of compounds **3**. The UV−vis absorption spectra of compounds **3ca** (**Si2′**), **3db**, and **3ec** are shown in Figure 1. The dichlorinated compound **3db**

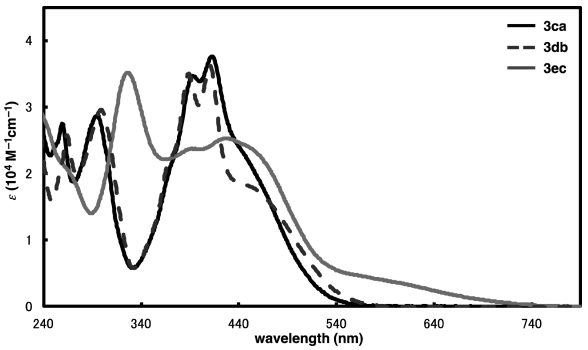

Figure 1. UV−vis spectra of compounds **3ca** (**Si2′**) (black line; at 2.4 × 10^{-5} M), **3db** (dark-gray broken line; at 2.8 × 10^{-5} M), and **3ec** (gray line; at 2.5 × 10^{-5} M) in CH_2Cl_2 at 25 °C.

exhibits a very similar absorption spectrum compared to the parent compound **3ca**, and the broad shoulder peak at around 470 nm mainly consists of the HOMO−LUMO transition in both cases on the basis of time-dependent density functional theory (TD-DFT) calculations.[10] In contrast, the introduction of dimethylamino and nitro groups at the two ends of the molecule significantly influenced its absorption spectrum. Thus, compound **3ec** shows absorbance up to ca. 740 nm, and this small but broad shoulder peak corresponds to the HOMO−LUMO transition according to the TD-DFT calculations, indicating that effective extension of the π-conjugation system was realized. Electrochemical analyses by cyclic voltammetry (CV) also gave consistent results (Table 2). Compared with

Table 2. Electrochemical Data for Compounds 3ca (Si2′), 3db, and 3ec

compound	$E_{ox}^{1/2}$ (V)[a,b]	$E_{red}^{1/2}$ (V)[a,c]	E_{HOMO} (eV)[d,e]	E_{LUMO} (eV)[e,f]
3ca (**Si2′**)	0.69	−1.96	−5.49 [−5.13]	−2.84 [−2.20]
3db	0.83	−1.77	−5.63 [−5.39]	−3.03 [−2.50]
3ec	0.17	−1.64	−4.97 [−4.90]	−3.16 [−2.52]

[a]Values are against Fc/Fc^+. [b]In CH_2Cl_2. [c]In THF. [d]$E_{HOMO} = -(4.8 + E_{ox}^{1/2})e$. [e]Values in brackets were calculated at the B3LYP/6-31G(d) level of theory.[11−13] [f]$E_{LUMO} = -(4.8 + E_{red}^{1/2})e$.

those of compound **3ca**, both the oxidation and reduction potentials became higher for **3db**, indicating that both the HOMO and LUMO levels became lower as a result of the introduction of chlorine atoms. On the basis of these CV data, the HOMO−LUMO energy gaps for **3ca** and **3db** are almost identical (2.65 and 2.60 eV, respectively), which is in good correlation with the observed UV−vis spectra for these compounds (Figure 1). On the other hand, the oxidation potential became lower and the reduction potential became higher for donor−acceptor-type compound **3ec**, as expected, leading to a narrower HOMO−LUMO energy gap (1.81 eV), which is also in good agreement with its UV−vis absorption spectrum as discussed above.

2-2. Comparison of Si1−Si6′. Here we obtained X-ray crystal structures of **Si2′** and **Si4′** in addition to the previously reported structures of **Si1**, **Si3**, and **Si5**, and the top views of these structures are compiled in Figure 2.[10,14] Although the terminal substituents are different for **Si2′** and **Si4′** (Me and *t*Bu in both cases), the core structures are almost symmetric, and Table 3 summarizes only the carbon−carbon bond lengths for the left-hand sides of the molecules. For all of these compounds, it was confirmed that the vertical carbon−carbon bonds (C1−C2, C3−C4, C5−C6, and C7−C8) are single bonds (1.470−1.488 Å) and the horizontal carbon−carbon bonds (C2−C3, C4−C5, C6−C7(C6′), and C8−C8′) are double bonds (1.356−1.380 Å), as expected by the bond-forming pathway of the stitching reaction. With regard to the planarity of the core structures, the torsion angles of the C_A-C_B and C_C-C_D bonds along C_B-C_C axis ($\angle C_AC_B-C_CC_D$) were calculated (Table 3). As is the case for **Si1**, newly synthesized **Si2′** and **Si4′** have highly planar π systems, which differ from the longer π systems with odd numbers of silole units (**Si3** and **Si5**), which show somewhat larger torsion angles of ca. 20°, although their structures still possess reasonably high planarity.[10] Overall, the stitched portions of all of these molecules are well-conjugated with alternating carbon−carbon single and double bonds that are effectively fixed in a plane by the bridging silicon atoms.

The UV−vis absorption spectra of these compounds are shown in Figure 3. The broad peaks at >400 nm are mainly attributable to HOMO−LUMO transitions according to the TD-DFT calculations,[10] and the molar absorption coefficient (ε) becomes larger in the order of increasing number of silole units. The maximum wavelength of absorbance in this region also becomes gradually longer in the same order, but the degree

DOI: 10.1021/jacs.7b00344
J. Am. Chem. Soc. 2017, 139, 3861−3867

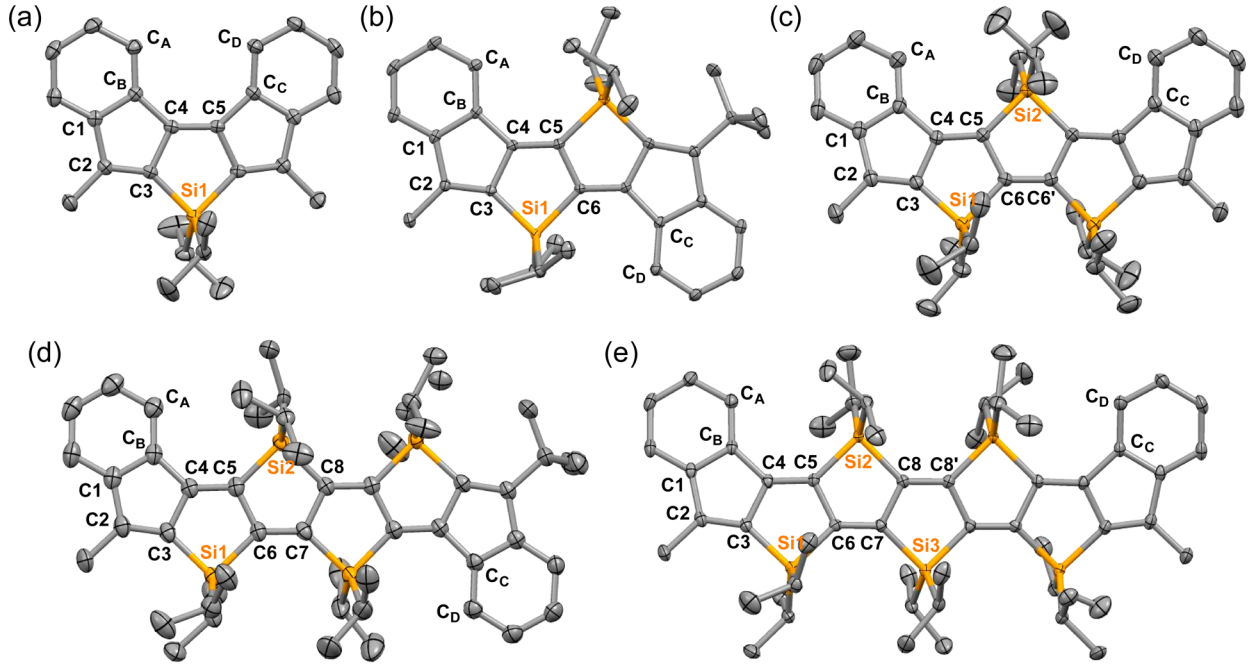

Figure 2. X-ray crystal structures of (a) **Si1**, (b) **Si2′**, (c) **Si3**, (d) **Si4′**, and (e) **Si5**. Hydrogen atoms have been omitted for clarity.

Table 3. Selected Bond Distances (Å) and Torsion Angles (deg) for Compounds Si1−Si5

	Si1	Si2′	Si3	Si4′	Si5
C1−C2	1.476(2)	1.472(2)	1.473(2)	1.470(5)	1.473(3)
C2−C3	1.356(2)	1.362(2)	1.361(2)	1.367(4)	1.358(3)
C3−C4	1.487(2)	1.485(2)	1.482(2)	1.480(4)	1.483(3)
C4−C5	1.368(2)	1.374(2)	1.373(2)	1.378(4)	1.365(3)
C5−C6	–	1.475(2)	1.478(2)	1.487(4)	1.488(3)
C6−C7(C6′)	–	–	1.375(2)	1.380(4)	1.375(3)
C7−C8	–	–	–	1.488(4)	1.482(3)
C8−C8′	–	–	–	–	1.375(4)
$\angle C_AC_B{-}C_CC_D$	4.8	2.8[a]	20.5	4.1[a]	19.9

[a] $180° - \angle C_AC_B{-}C_CC_D$.

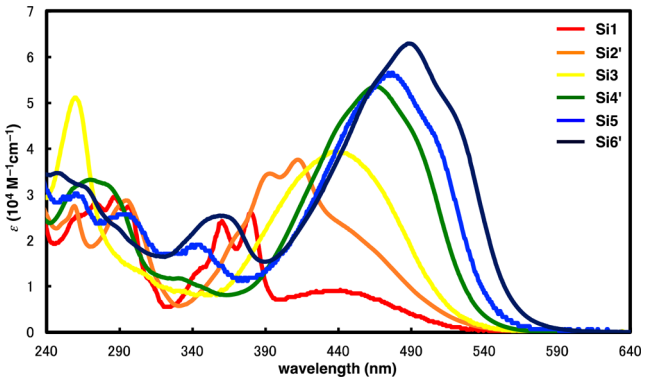

Figure 3. UV−vis spectra of compounds **Si1** (red line; at 3.8×10^{-6} M), **Si2′** (orange line; at 2.4×10^{-5} M), **Si3** (yellow line; at 4.2×10^{-6} M), **Si4′** (green line; at 2.5×10^{-5} M), **Si5** (blue line; at 1.5×10^{-6} M), and **Si6′** (indigo blue line; at 2.3×10^{-5} M) in CH_2Cl_2 at 25 °C.

of red shift is relatively small, with only a 47 nm difference between **Si1** (442 nm) and **Si6′** (489 nm) at the peak tops; the difference in absorption-edge wavelengths is also quite small, despite the fact that **Si6′** is longer than **Si1** by five alkene units (10 π electrons). For comparison, the UV−vis absorption spectra of (*E*)-stilbene, (1*E*,3*E*)-1,4-diphenyl-1,3-butadiene, and (1*E*,3*E*,5*E*)-1,6-diphenyl-1,3,5-hexatriene are compiled in Figure 4 as an example of a typical extended π-conjugation system, which shows a red shift of ca. 30 nm for each alkene extension. These different trends clearly indicate that, unlike the typical extended π-conjugation system, the HOMO−

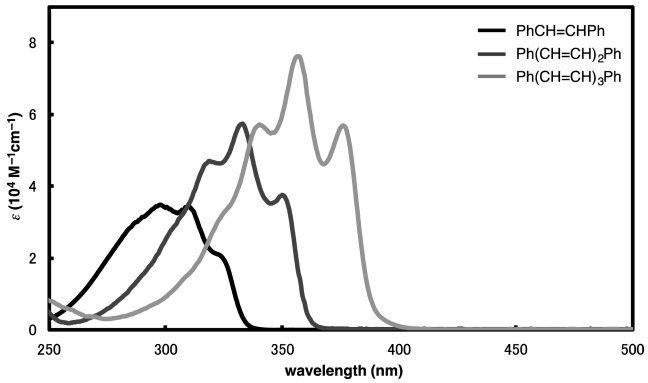

Figure 4. UV−vis spectra of (*E*)-stilbene (black line; at 8.3×10^{-5} M), (1*E*,3*E*)-1,4-diphenyl-1,3-butadiene (dark-gray line; at 7.8×10^{-6} M), and (1*E*,3*E*,5*E*)-1,6-diphenyl-1,3,5-hexatriene (light-gray line; at 8.6×10^{-6} M) in CH_2Cl_2 at 25 °C.

DOI: 10.1021/jacs.7b00344
J. Am. Chem. Soc. 2017, 139, 3861−3867

LUMO gaps do not become significantly narrower in going from **Si1** to **Si6′** in this series of quinoidal fused oligosiloles.[15] This trend is also confirmed by the electrochemical analysis, as discussed below. With regard to the emission properties, none of these quinoidal fused oligosiloles showed photoluminescence, unlike other silicon-bridged π-conjugated compounds such as dibenzosiloles and bis-silicon-bridged stilbene homologues.[1,4]

A comparison of the electrochemical data for these compounds obtained using cyclic voltammetry is summarized in Table 4. Both the oxidation and reduction potentials of

Table 4. Electrochemical Data for Compounds Si1−Si6′

compound	$E_{ox}^{1/2}$ (V)[a,b]	$E_{red}^{1/2}$ (V)[a,c]	E_{HOMO} (eV)[d,e]	E_{LUMO} (eV)[e,f]
Si1	0.90	−1.90	−5.70 [−5.36]	−2.90 [−2.22]
Si2′	0.69	−1.96	−5.49 [−5.15][g]	−2.84 [−2.19][g]
Si3	0.55	−2.01	−5.35 [−4.99]	−2.79 [−2.15]
Si4′	0.40	−2.04	−5.20 [−4.88][h]	−2.76 [−2.14][h]
Si5	0.34	−2.07	−5.14 [−4.80]	−2.73 [−2.11]
Si6′	0.24	−2.11	−5.04 [−4.75][i]	−2.69 [−2.13][i]

[a]Values are against Fc/Fc^+. [b]In CH_2Cl_2. [c]In THF. [d]$E_{HOMO} = -(4.8 + E_{ox}^{1/2})e$. [e]Values in brackets were calculated at the B3LYP/6-31G(d) level of theory. [f]$E_{LUMO} = -(4.8 + E_{red}^{1/2})e$. [g]Calculated for **Si2**. [h]Calculated for **Si4** (*t*Bu on **Si4′** was replaced by Me). [i]Calculated for **Si6** (*t*Bu on **Si6′** was replaced by Me).

newly obtained **Si2′** are between those of **Si1** and **Si3**. The same trend was observed for **Si4′** compared with **Si3** and **Si5**, and **Si6′** showed lower oxidation and reduction potentials than **Si5**. In overall, both the oxidation and reduction potentials become lower in the order of **Si1**, **Si2′**, **Si3**, **Si4′**, **Si5**, and **Si6′**, indicating that not only the HOMO level but also the LUMO level become higher for the longer π-conjugation system, which is a very unusual phenomenon.[16] This unusual trend in the LUMO levels was mostly reproduced by the DFT calculations, as shown by the values in brackets in Table 4, which led us to investigate its origin through computational studies in detail, as described in the following section.

3. Computational Investigation of the Origin of the Frontier Orbital Energy Profiles. As shown in Table 4 (Section 2-2), while the HOMO levels of these quinoidal fused oligosiloles become higher in the order of **Si1**−**Si6′**, the LUMO levels also gradually become higher in this order. To understand the origin of this unusual LUMO trend, we decided to perform several theoretical calculations. According to the frontier orbital profiles for **Si1**−**Si6** (Figure 5), the contributions of the silicon-bridge moieties to the HOMOs and LUMOs are very minute. Indeed, when we cleaved these silicon bridges and replaced them by C−H bonds while maintaining the overall geometries (**H1**−**H6**; Figure 6) for single-point

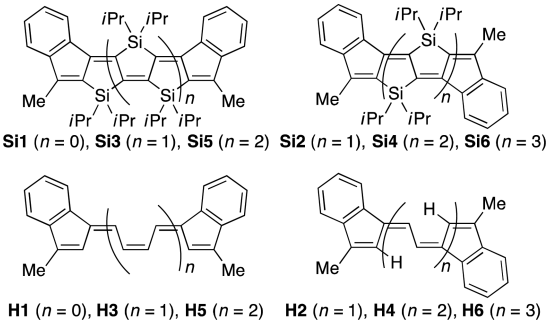

Figure 6. Structures of **Si1**−**Si6** and unbridged **H1**−**H6**.

DFT calculations, very similar energy profiles were obtained, indicating that the silicon bridges in **Si1**−**Si6** are not primarily responsible for the observed HOMO/LUMO trends (Table 5).

To gain more insights into the relationship between the structures and energy profiles, we examined model compounds **Si1a**−**Si6a** and **Si1b**−**Si6b**, whose terminal structures are cyclopentadienylidenes and linear alkenes, respectively, instead of original indenylidenes (Figure 7). The structures were optimized by DFT calculations[11] at the B3LYP/6-31G(d) level of theory[12,13] to elucidate their frontier orbital energies. As shown in Tables 6 and 7, while **Si1a**−**Si6a** exhibit a trend similar to that of the parents **Si1**−**Si6** (higher HOMO and

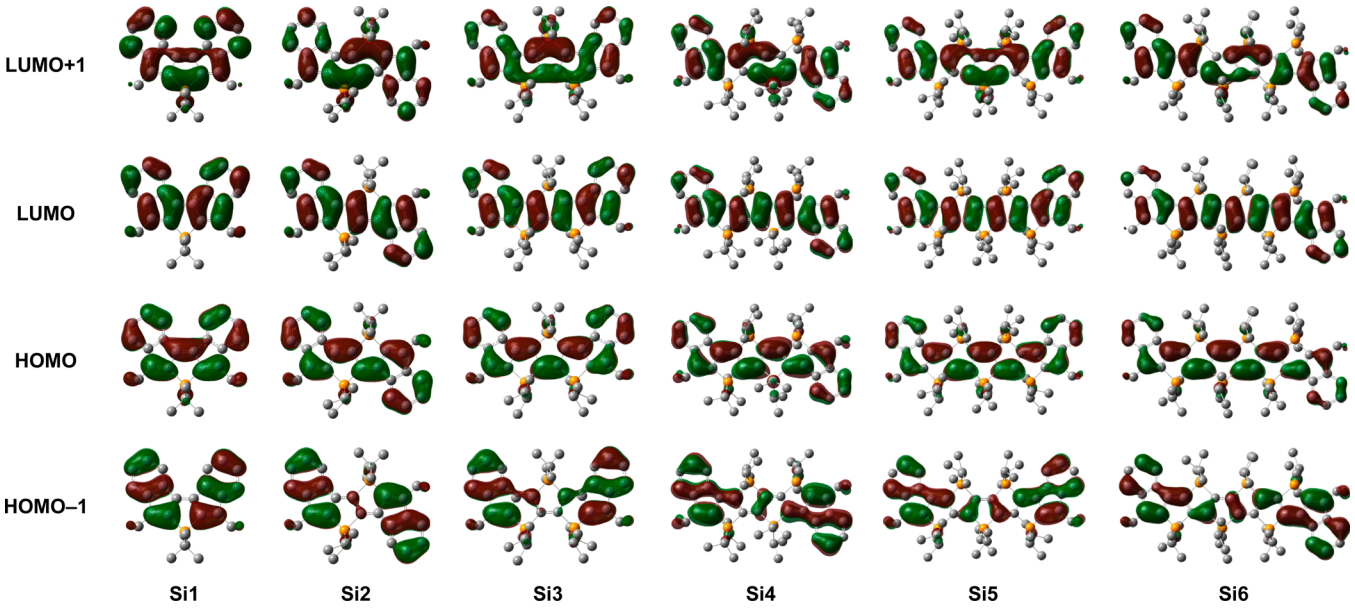

Figure 5. Calculated frontier orbital profiles of **Si1**−**Si6**.

DOI: 10.1021/jacs.7b00344
J. Am. Chem. Soc. 2017, 139, 3861−3867

Table 5. Calculated Frontier Orbital Energies of Si1−Si6 and H1−H6

cmpd	E_{HOMO} (eV)[a]	E_{LUMO} (eV)[a]	cmpd	E_{HOMO} (eV)[b]	E_{LUMO} (eV)[b]
Si1	−5.36	−2.22	**H1**	−5.43 (−5.34)	−2.23 (−2.31)
Si2	−5.15	−2.19	**H2**	−5.28 (−5.26)	−2.20 (−2.40)
Si3	−4.99	−2.15	**H3**	−5.17 (−5.15)	−2.16 (−2.46)
Si4	−4.88	−2.14	**H4**	−5.08 (−5.06)	−2.12 (−2.50)
Si5	−4.80	−2.11	**H5**	−5.02 (−4.98)	−2.09 (−2.53)
Si6	−4.75	−2.13	**H6**	−4.98 (−4.93)	−2.09 (−2.55)

[a]Calculated at the B3LYP/6-31G(d) level of theory with structural optimization. [b]Calculated at the B3LYP/6-31G(d) level of theory using the optimized structures for **Si1−Si6**. Values in parentheses are calculated at the B3LYP/6-31G(d) level of theory with structural optimization (**H1opt−H6opt**).

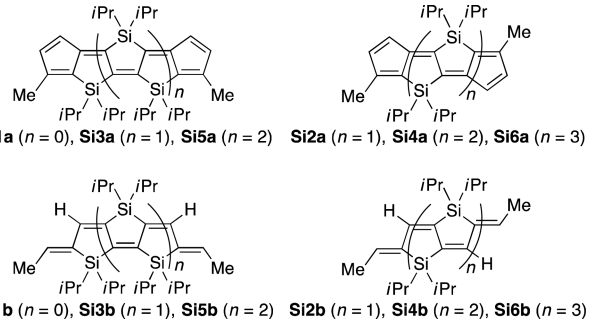

Si1a (*n* = 0), **Si3a** (*n* = 1), **Si5a** (*n* = 2) **Si2a** (*n* = 1), **Si4a** (*n* = 2), **Si6a** (*n* = 3)

Si1b (*n* = 0), **Si3b** (*n* = 1), **Si5b** (*n* = 2) **Si2b** (*n* = 1), **Si4b** (*n* = 2), **Si6b** (*n* = 3)

Figure 7. Structures of **Si1a−Si6a** and **Si1b−Si6b**.

Table 6. Calculated Frontier Orbital Energies of Si1a−Si6a and H1a−H6a

cmpd	E_{HOMO} (eV)[a]	E_{LUMO} (eV)[a]	cmpd	E_{HOMO} (eV)[b]	E_{LUMO} (eV)[b]
Si1a	−5.62	−2.45	**H1a**	−5.60	−2.41
Si2a	−5.56	−2.36	**H2a**	−5.65	−2.37
Si3a	−5.36	−2.32	**H3a**	−5.55	−2.32
Si4a	−5.16	−2.26	**H4a**	−5.38	−2.25
Si5a	−4.99	−2.22	**H5a**	−5.25	−2.21
Si6a	−4.88	−2.20	**H6a**	−5.16	−2.19

[a]Calculated at the B3LYP/6-31G(d) level of theory with structural optimization. [b]Calculated at the B3LYP/6-31G(d) level of theory using the optimized structures for **Si1a−Si6a**.

Table 7. Calculated Frontier Orbital Energies of Si1b−Si6b and H1b−H6b

cmpd	E_{HOMO} (eV)[a]	E_{LUMO} (eV)[a]	cmpd	E_{HOMO} (eV)[b]	E_{LUMO} (eV)[b]
Si1b	−5.20	−0.69	**H1b**	−5.25	−0.67
Si2b	−4.94	−0.99	**H2b**	−5.04	−0.93
Si3b	−4.79	−1.22	**H3b**	−4.91	−1.10
Si4b	−4.72	−1.43	**H4b**	−4.85	−1.23
Si5b	−4.65	−1.56	**H5b**	−4.79	−1.34
Si6b	−4.56	−1.65	**H6b**	−4.73	−1.43

[a]Calculated at the B3LYP/6-31G(d) level of theory with structural optimization. [b]Calculated at the B3LYP/6-31G(d) level of theory using the optimized structures for **Si1b−Si6b**.

LUMO levels for longer π conjugation), for **Si1b−Si6b** the LUMO levels become lower as the π conjugation is extended, as is the case for regular extended π systems. For comparison, we also removed the silicon bridges in both of these series while retaining the overall geometries to generate **H1a−H6a** and **H1b−H6b** (Figure 8), respectively, and assessed their energy

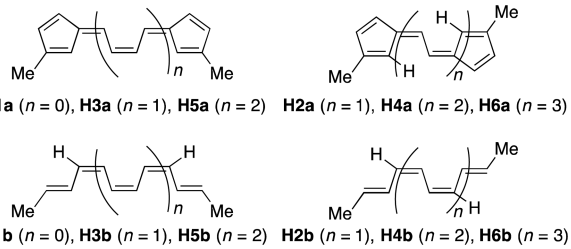

H1a (*n* = 0), **H3a** (*n* = 1), **H5a** (*n* = 2) **H2a** (*n* = 1), **H4a** (*n* = 2), **H6a** (*n* = 3)

H1b (*n* = 0), **H3b** (*n* = 1), **H5b** (*n* = 2) **H2b** (*n* = 1), **H4b** (*n* = 2), **H6b** (*n* = 3)

Figure 8. Structures of **H1a−H6a** and **H1b−H6b**.

profiles by single-point DFT calculations. **H1a−H6a** showed a trend similar to that for **Si1a−Si6a** (i.e., higher HOMO and LUMO levels for longer π conjugation; Table 6), whereas **H1b−H6b** reproduced the trend of **Si1b−Si6b** (i.e., higher HOMO and lower LUMO levels for longer π conjugation; Table 7). These results strongly suggest that the unusual trend observed for the LUMO levels in **Si1−Si6** mostly originates from the terminal indenylidene structures (or cyclopentadienylidenes for **Si1a−Si6a**) of the silicon-bridged polyenes.

To evaluate the effect of geometrical constraints caused by the silicon bridges, **H1−H6** generated from **Si1−Si6** and structurally optimized **H1−H6** (**H1opt−H6opt**) were also compared. As discussed above, the LUMO levels became higher in **H1−H6** for longer π conjugation (Table 5), but **H1opt−H6opt** exhibited slight lowering of the LUMO levels upon extension of the π conjugation (a decrease of 0.24 eV in going from **H1opt** to **H6opt**; Table 5, values in parentheses), indicating that subtle geometrical differences can also affect the overall electronic properties.[10] In this regard, the silicon bridges are considered to play a positive role in the observed trend in the LUMO levels by fixing the geometry of these compounds, but the contribution of the terminal indenylidene (or cyclopentadienylidene) structures is much larger, as shown by comparison of Tables 5−7 (e.g., a decrease of 0.96 eV in going from **Si1b** to **Si6b**, which lack terminal indenylidenes/cyclopentadienylidenes).

On the basis of the above considerations, we decided to further simplify the structures to **H1′−H6′** or **H1a′−H6a′** (Figure 9) and examine how the terminal structures affect the

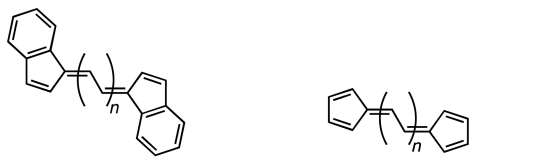

H1' (*n* = 0), **H2'** (*n* = 1), **H3'** (*n* = 2) **H1a'** (*n* = 0), **H2a'** (*n* = 1), **H3a'** (*n* = 2)
H4' (*n* = 3), **H5'** (*n* = 4), **H6'** (*n* = 5) **H4a'** (*n* = 3), **H5a'** (*n* = 4), **H6a'** (*n* = 5)

Figure 9. Structures of **H1′−H6′** and **H1a′−H6a′**.

frontier orbital energies in view of π electrons using Hückel calculations.[10] This simplified analysis of the π system strongly suggested that the existence of indenylidene (cyclopentadienylidene) moieties at each end of **Si1−Si6** (**Si1a−Si6a**) mainly controls the LUMO levels by mixing the frontier orbitals of these terminal units with the HOMO of the central polyene unit. Because the HOMO level of the polyene becomes higher with longer conjugation, the overall LUMO level becomes higher with longer π conjugation for **Si1−Si6**.

DOI: 10.1021/jacs.7b00344
J. Am. Chem. Soc. 2017, 139, 3861−3867

CONCLUSIONS

We newly synthesized quinoidal fused oligosiloles containing an even number of silole units by a rhodium-catalyzed stitching reaction. Employing $[RhCl(tfb)]_2$ as the catalyst significantly improved the stitching efficiency, and up to six siloles could be fused in quinoidal form. Through a systematic comparison of the physical properties of **Si1**−**Si6′**, we confirmed the unique trend in their LUMO levels, which become higher with longer π conjugation. To understand the origin of this unusual trend, we also carried out theoretical calculations using various model compounds, and the results indicated that the terminal indenylidene (cyclopentadienylidene) moieties in **Si1**−**Si6** (**Si1a**−**Si6a**) are primarily responsible for this phenomenon through their frontier orbital correlations with the HOMO of the central polyene unit, which becomes higher in energy with longer conjugation.

ASSOCIATED CONTENT

Supporting Information

The Supporting Information is available free of charge on the ACS Publications website at DOI: 10.1021/jacs.7b00344.

Experimental procedures, characterization data, crystallographic data, cyclic voltammograms, computational procedures and results, NMR spectra, and complete ref 11 (as SI ref 7) (PDF)

Crystallographic data for **3ca** (**Si2′**) (CIF)

Crystallographic data for **Si4′** (CIF)

AUTHOR INFORMATION

Corresponding Authors

*shintani@chembio.t.u-tokyo.ac.jp

*yamasita@chemsys.t.u-tokyo.ac.jp

*nozaki@chembio.t.u-tokyo.ac.jp

ORCID

Ryo Shintani: 0000-0002-3324-9393

Kyoko Nozaki: 0000-0002-0321-5299

Author Contributions

§N.M. and T.T. contributed equally.

Notes

The authors declare no competing financial interest.

ACKNOWLEDGMENTS

Support was provided in part by a Grant-in-Aid for Challenging Exploratory Research (MEXT, Japan), the JGC-S Scholarship Foundation, and the Asahi Glass Foundation. We thank Dr. Shingo Ito and Dr. Shuhei Kusumoto at The University of Tokyo for help with X-ray crystallographic analysis.

REFERENCES

(1) For reviews, see: (a) Chen, J.; Cao, Y. *Macromol. Rapid Commun.* **2007**, *28*, 1714. (b) Wong, W. W. H.; Hooper, J. F.; Holmes, A. B. *Aust. J. Chem.* **2009**, *62*, 393. (c) Fu, H.; Cheng, Y. *Curr. Org. Chem.* **2012**, *16*, 1423.

(2) For reviews, see: (a) Ohshita, J. *Macromol. Chem. Phys.* **2009**, *210*, 1360. (b) Beaujuge, P. M.; Amb, C. M.; Reynolds, J. R. *Acc. Chem. Res.* **2010**, *43*, 1396. (c) Facchetti, A. *Chem. Mater.* **2011**, *23*, 733. (d) Son, H. J.; Carsten, B.; Jung, I. H.; Yu, L. *Energy Environ. Sci.* **2012**, *5*, 8158. (e) Coughlin, J. E.; Henson, Z. B.; Welch, G. C.; Bazan, G. C. *Acc. Chem. Res.* **2014**, *47*, 257.

(3) For an early example, see: Ishikawa, M.; Tabohashi, T.; Sugisawa, H.; Nishimura, K.; Kumada, M. *J. Organomet. Chem.* **1983**, *250*, 109.

(4) (a) Yamaguchi, S.; Xu, C.; Tamao, K. *J. Am. Chem. Soc.* **2003**, *125*, 13662. (b) Xu, C.; Yamada, H.; Wakamiya, A.; Yamaguchi, S.; Tamao, K. *Macromolecules* **2004**, *37*, 8978. (c) Yamaguchi, S.; Tamao, K. *Chem. Lett.* **2005**, *34*, 2. (d) Yamada, H.; Xu, C.; Fukazawa, A.; Wakamiya, A.; Yamaguchi, S. *Macromol. Chem. Phys.* **2009**, *210*, 904. Also see: (e) Toulokhonova, I. S.; Stringfellow, T. C.; Ivanov, S. A.; Masunov, A.; West, R. *J. Am. Chem. Soc.* **2003**, *125*, 5767.

(5) Shintani, R.; Iino, R.; Nozaki, K. *J. Am. Chem. Soc.* **2016**, *138*, 3635.

(6) For a related synthetic approach under palladium catalysis, see: (a) Zhao, J.; Oniwa, K.; Asao, N.; Yamamoto, Y.; Jin, T. *J. Am. Chem. Soc.* **2013**, *135*, 10222. (b) Luo, Y.; Pan, X.; Wu, J. *Org. Lett.* **2011**, *13*, 1150. (c) Luo, Y.; Hong, L.; Wu, J. *Chem. Commun.* **2011**, *47*, 5298. Also see: (d) Levi, Z. U.; Tilley, T. D. *J. Am. Chem. Soc.* **2009**, *131*, 2796.

(7) For the synthesis of structurally related quinoidal fused oligothiophenes and selenophenes by a stepwise approach, see: (a) Rudebusch, G. E.; Fix, A. G.; Henthorn, H. A.; Vonnegut, C. L.; Zakharov, L. N.; Haley, M. M. *Chem. Sci.* **2014**, *5*, 3627. (b) Shi, X.; Burrezo, P. M.; Lee, S.; Zhang, W.; Zheng, B.; Dai, G.; Chang, J.; López Navarrete, J. T.; Huang, K.-W.; Kim, D.; Casado, J.; Chi, C. *Chem. Sci.* **2014**, *5*, 4490. (c) Marshall, J. L.; Rudebusch, G. E.; Vonnegut, C. L.; Zakharov, L. N.; Haley, M. M. *Tetrahedron Lett.* **2015**, *56*, 3235.

(8) Takahashi, K.; Ito, S.; Shintani, R.; Nozaki, K. *Chem. Sci.* **2017**, *8*, 101.

(9) Rh/tfb complexes are known to be effective catalysts for polymerization of arylacetylenes. See: (a) Saeed, I.; Shiotsuki, M.; Masuda, T. *Macromolecules* **2006**, *39*, 8977. (b) Onishi, N.; Shiotsuki, M.; Sanda, F.; Masuda, T. *Macromolecules* **2009**, *42*, 4071. (c) Nishimura, T.; Ichikawa, Y.; Hayashi, T.; Onishi, N.; Shiotsuki, M.; Masuda, T. *Organometallics* **2009**, *28*, 4890.

(10) See the Supporting Information for details.

(11) Calculations were performed using Gaussian 09: Frisch, M. J.; et al. *Gaussian 09*, revision D.01; Gaussian, Inc.: Wallingford, CT, 2013.

(12) (a) Lee, C.; Yang, W.; Parr, R. G. *Phys. Rev. B: Condens. Matter Mater. Phys.* **1988**, *37*, 785. (b) Becke, A. D. *J. Chem. Phys.* **1993**, *98*, 5648.

(13) (a) Ditchfield, R.; Hehre, W. J.; Pople, J. A. *J. Chem. Phys.* **1971**, *54*, 724. (b) Hehre, W. J.; Ditchfield, R.; Pople, J. A. *J. Chem. Phys.* **1972**, *56*, 2257.

(14) CCDC-1524493 and CCDC-1524494 contain the supplementary crystallographic data for this paper. These data can be obtained free of charge from the Cambridge Crystallographic Data Centre via www.ccdc.cam.ac.uk/data_request/cif.

(15) Structurally related quinoidal fused oligothiophenes show a 123 nm red shift in their longest absorption maxima in going from the compound containing two sulfurs (606 nm) to the one containing four sulfurs (729 nm), although the compound containing one sulfur behaves differently. See ref 7b for details.

(16) [*n*]Cycloparaphenylenes are known to exhibit lower HOMO and higher LUMO levels as the number of rings (*n*) increases. This is due to the strain-induced quinoidal contribution for smaller rings. See: (a) Iwamoto, T.; Watanabe, Y.; Sakamoto, Y.; Suzuki, T.; Yamago, S. *J. Am. Chem. Soc.* **2011**, *133*, 8354. (b) Kayahara, E.; Kouyama, T.; Kato, T.; Yamago, S. *J. Am. Chem. Soc.* **2016**, *138*, 338.

DOI: 10.1021/jacs.7b00344
J. Am. Chem. Soc. 2017, 139, 3861−3867